

Electronic Supplementary Information

Experimental section

Materials: Perylene-3,4,9,10-tetracarboxylic dianhydride (PTCDA, 97%), Nafion (5 wt%) solution, salicylic acid, sodium citrate, salicylate ($C_7H_6O_3$), sodium hypochlorite ($NaClO$), sodium nitroferricyanide ($C_5FeN_6Na_2O$), ammonium chloride (NH_4Cl), sodium hydroxide ($NaOH$), sodium sulfate (Na_2SO_4), carbon paper (CP; TGP-H-060), and para-(dimethylamino) benzaldehyde ($C_9H_{11}NO$) were purchased from Beijing Chemical Corporation. Hydrochloric acid (HCl) and ethanol were purchased from Aladdin Ltd. (Shanghai, China). All reagents were analytical reagent grade and used as received without further purification. Nafion 117 membrane (DuPont) was purchased from HESSEN Co., Ltd. (Shanghai, China). Ultrapure water used throughout all experiments was purified through a Millipore system.

Preparation of PTCA-rGO: Graphene oxide (GO) was synthesized by a modified Hummer's method and then calcinated in Ar at 700 °C with heating rate of 5 °C min⁻¹ for 1 h to obtain rGO. The perylene-3,4,9,10-tetracarboxylic acid (PTCA) was made by hydrolyzing PTCDA. Briefly, 0.1 g PTCDA was dissolved in an appropriate amount of 1.0 M NaOH. Then 1.0 M HCl was dropped gradually into the mixture solution and red deposits appeared in the yellow-green solution. Until precipitated completely, the prepared PTCA were collected by centrifugation, washed with ultrapure water and dried under vacuum at room temperature. 30 mg rGO and 30 mg PTCA dissolved in 30.0 mL water by ultrasonication, and then collected by centrifugation, washed with ultrapure water and dried under vacuum at 40 °C overnight.

Preparation of PTCA-rGO/CP: Carbon paper (CP) was cleaned via brief sonication with ethanol and water for several times. To prepare the PTCA-rGO ink, 5 mg PTCA-

rGO and 40 μL 5 wt% Nafion solution were dispersed in 960 μL water/ethanol (V : V = 1 : 3) followed by 3-h sonication to form a homogeneous ink. Then, 20 μL ink was loaded onto the CP ($1 \times 1 \text{ cm}^2$) and dried under ambient condition. The PTCA-rGO/CP working electrode was prepared well.

Characterizations: TEM images were collected on a transmission electron microscopy (HITACHI H-8100, Tokyo, Japan). XPS measurements were performed on an ESCALABMK II X-ray photoelectron spectrometer using Mg as the exciting source. The absorbance data of spectrophotometer were acquired on SHIMADZU UV-1800 UV-Vis spectrophotometer. A gas chromatograph (SHIMADZU, GC-2014C) equipped with MolSieve 5A column and Ar carrier gas was used for H_2 quantifications. Gas-phase product was sampled every 600 s using a gas-tight syringe (Hamilton).

Electrochemical measurements: N_2 reduction experiments were carried out in a two-compartment cell under ambient condition, which was separated by Nafion 117 membrane. The membrane was protonated by first boiling in ultrapure water for 1 h and treating in H_2O_2 (5 wt%) aqueous solution at 80 $^\circ\text{C}$ for another 1 h, respectively. And then, the membrane was treated in 0.5 M H_2SO_4 for 3 h at 80 $^\circ\text{C}$ and finally in water for 6 h. The electrochemical experiments were carried out with an electrochemical workstation (CHI 660E) using a three-electrode configuration with prepared electrodes, graphite rod and Ag/AgCl electrode (saturated KCl electrolyte) as working electrode, counter electrode and reference electrode, respectively. The potentials reported in this work were converted to reversible hydrogen electrode (RHE) scale via calibration with the following equation: $E (\text{vs. RHE}) = E (\text{vs. Ag/AgCl}) + 0.059 \times \text{pH} + 0.197 \text{ V}$ and the presented current density was normalized to the

geometric surface area. For electrochemical N₂ reduction, chrono-amperometry tests were conducted in N₂-saturated 0.1 M HCl solution (30 mL).

Determination of NH₃: Concentration of produced NH₃ was spectrophotometrically determined by the indophenol blue method.¹ In detail, 2 mL of post-tested solution was got from the electrochemical reaction vessel. Then, 2 mL of 1 M NaOH solution (contains 5 wt% salicylic acid and 5 wt% sodium citrate) was followed by addition of 1 mL of 0.05 M sodium hypochlorite and 0.2 mL of sodium nitroferricyanide (1 wt%). After standing at 25 °C for 2 h, the UV-Vis absorption spectrum was measured. The concentration of indophenol blue was determined using the absorbance at wavelength of 655 nm. The concentration-absorbance curve was calibrated using the standard NH₄Cl solution with NH₃ concentrations of 0.0, 0.05, 0.10, 0.15, 0.20, 0.30, and 0.40 μg mL⁻¹ in 0.1 M HCl. Typically, 100 μg mL⁻¹ NH₃ solution was prepared (0.158 g NH₄Cl dissolved in 500 mL 0.1 M HCl) and diluted to 1 μg mL⁻¹. Then, 0.0, 0.1, 0.2, 0.3, 0.4, 0.6, and 0.8 mL NH₃ solution with concentration of 1 μg mL⁻¹ were poured into test tubes and separately diluted to 2 mL with 0.1 M HCl and the resulting concentrations of NH₃ in the solutions are 0.0, 0.05, 0.10, 0.15, 0.20, 0.30, and 0.40 μg mL⁻¹. The fitting curve ($y = 0.393 x + 0.043$, $R^2 = 0.999$) shows good linear relation of absorbance value with NH₃ concentration by three times independent calibrations.

Determination of N₂H₄: The N₂H₄ possibly was estimated by the method of Watt and Chrisp.² A mixed solution of 5.99 g C₉H₁₁NO, 30 mL concentrated HCl and 300 ml ethanol was used as a color reagent. Calibration curve was plotted as follow: firstly, preparing a series of N₂H₄ solutions of known concentration as standards; secondly, adding 5 mL color reagent to above N₂H₄ solution, separately, and standing 20 min at room temperature; finally, the absorbance of the resulting solution was measured at

460 nm. The fitting curve shows good linear relation of absorbance with $\text{N}_2\text{H}_4\cdot\text{H}_2\text{O}$ concentration ($y = 0.881 x + 0.033$, $R^2 = 0.999$) by three times independent calibrations.

Determination of FE and NH_3 yield: The FE for N_2 reduction was defined as the amount of electric charge used for synthesizing NH_3 divided the total charge passed through the electrodes during the electrolysis. The total amount of NH_3 produced was measured using colorimetric methods. Assuming three electrons were needed to produce one NH_3 molecule, the FE could be calculated as follows:

$$\text{FE}(\text{NH}_3) = 3 \times F \times [\text{NH}_3] \times V / (17 \times Q) \times 100\%$$

The rate of NH_3 formation was calculated using the following equation:

$$\text{NH}_3 \text{ yield} = [\text{NH}_3] \times V / (m_{\text{cat.}} \times t)$$

The amount of NH_3 was calculated as follows:

$$m_{\text{NH}_3} = [\text{NH}_3] \times V$$

Where F is the Faraday constant, $[\text{NH}_3]$ is the measured NH_3 concentration, V is the volume of the electrolyte in the cathodic chamber, Q is the total quantity of applied electricity, t is the reduction time, and $m_{\text{cat.}}$ is the loaded mass of catalyst on carbon paper.

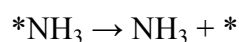
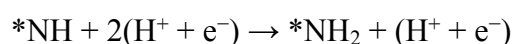
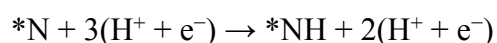
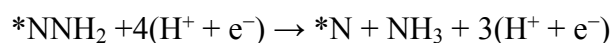
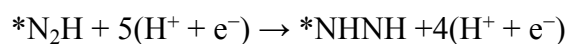
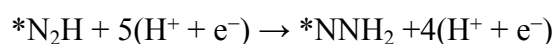
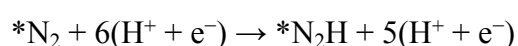
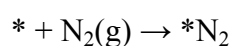
The FE of H_2 was calculated as below:

$$\text{FE}(\text{H}_2) = 2 \times F V_{\text{H}_2} \times G \times p_0 / (R \times T \times Q) \times 100\%$$

Where V_{H_2} is the volume concentration of H_2 in the exhaust gas from the electrochemical cell (GC data), G is the gas flow rate (mL min^{-1}), Q is the total quantity of applied electricity, $p_0 = 1.01 \times 10^5 \text{ Pa}$, $T = 298.15 \text{ K}$, and $R = 8.314 \text{ J mol}^{-1} \text{ K}^{-1}$.

Computational Details: The density functional theory (DFT) calculations are performed using the projector augmented wave and generalized gradient

approximation in the form of the Perdew-Burke-Ernzerh of exchange-correlation functional,^{3,4} as implemented in the Vienna Ab Initio Simulation Package (VASP).⁵⁻⁷ The van der Waals interaction is described using the empirical correction scheme of Grimme. In our calculated slab models, an 8×8 two-dimensional graphene supercell with one carbon vacancy as a model of rGO has been used. One PTCA molecular is physically absorbed on the rGO surface. In DFT calculations, the energy cutoffs of plane wave for carbon, hydrogen, oxygen, and nitrogen are selected as 500 eV. A vacuum layer of 25 Å is added to avoid the interaction between nearby supercells. Then the structures are fully optimized until the following convergence criteria are reached: 10⁻⁴ eV for atomic energy and -0.02 eV Å⁻¹ of atomic force. In NRR processes, the anode reaction i.e. H₂ ↔ 2(H⁺ + e⁻) is taken as a convenient reference, which works as the source of proton and electrons. Six net proton coupled electron transfer steps (N₂ + 6H⁺ + 6e⁻ → NH₃) are involved, There are several steps following associative mechanism where the nitrogen molecular are hydrogenated by protons (an asterisk,* , denotes a site on the surface).



Another dissociative mechanism, where the nitrogen molecules are first dissociated on the surface, is not discussed here because it is hard to occur under our experimental temperature and pressure.

The Gibbs free energy change (ΔG) of every elemental step is calculated by using the RHE model proposed by Nørskov et al.⁸ and they approximate the chemical potential of a proton-electron pair with a half of chemical potential of hydrogen molecule. The free energy change is defined as $\Delta G = \Delta E + \Delta ZPE - T\Delta S + \Delta G_U$, where ΔE is the reaction energy directly obtained from DFT calculations; ΔZPE is the change in zero-point energy; T is temperature (298.15 K); ΔS is the change in entropy. $\Delta G_U = -neU$, where n is the number of electrons transferred and U is the electrode potential. The zero-point energies and entropies of the NRR species are determined from the vibrational frequencies in which only the adsorbed species' vibrational modes are computed explicitly and the electrocatalyst sheet is fixed. The entropies and vibrational frequencies of gas phase molecules are taken from the NIST database.⁹

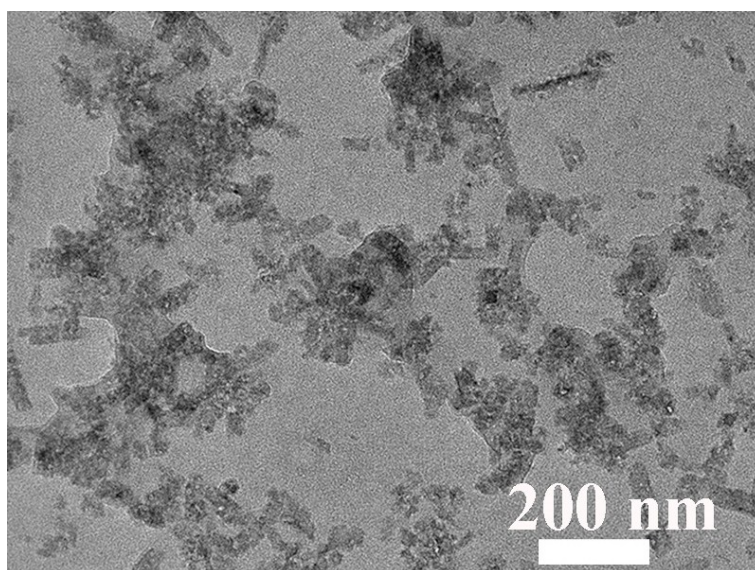


Fig. S1. TEM image of PTCA.

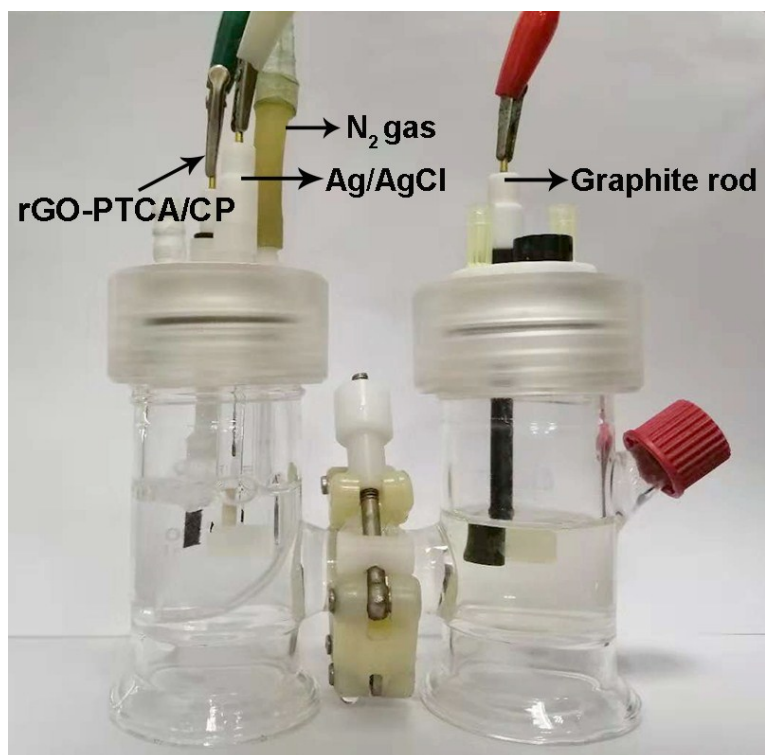


Fig. S2. Optical photograph of the two-compartment electrochemical cell.

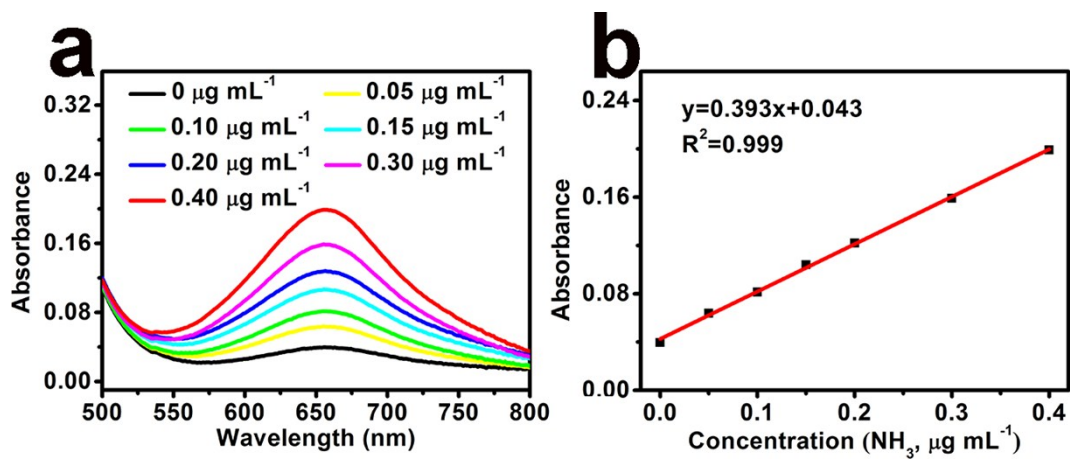


Fig. S3. (a) UV-Vis absorption spectra of NH_3 concentrations after incubated for 2 h at room temperature. (b) Calibration curve used for calculation of NH_3 concentrations.

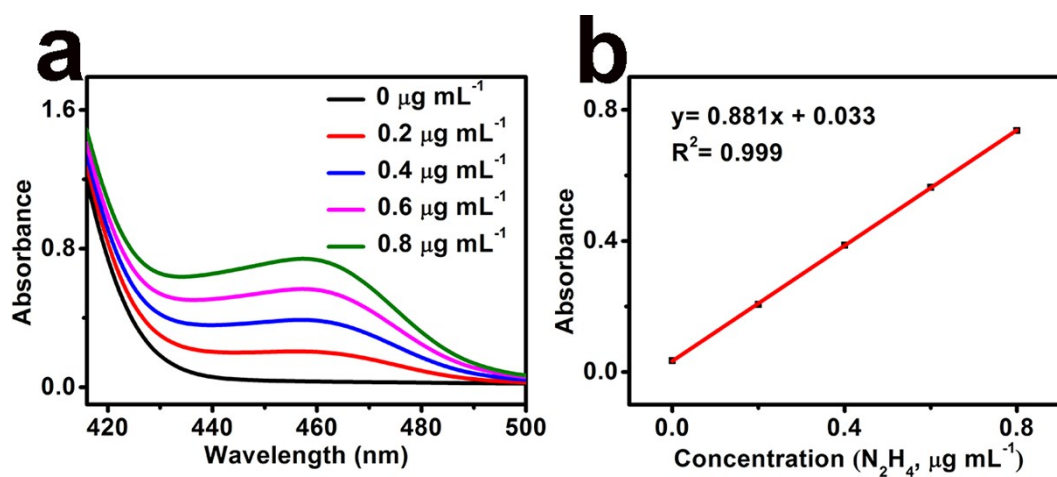


Fig. S4. (a) UV-Vis absorption spectra of N_2H_4 concentrations after incubated for 20 min at room temperature. (b) Calibration curve used for calculation of N_2H_4 concentrations.

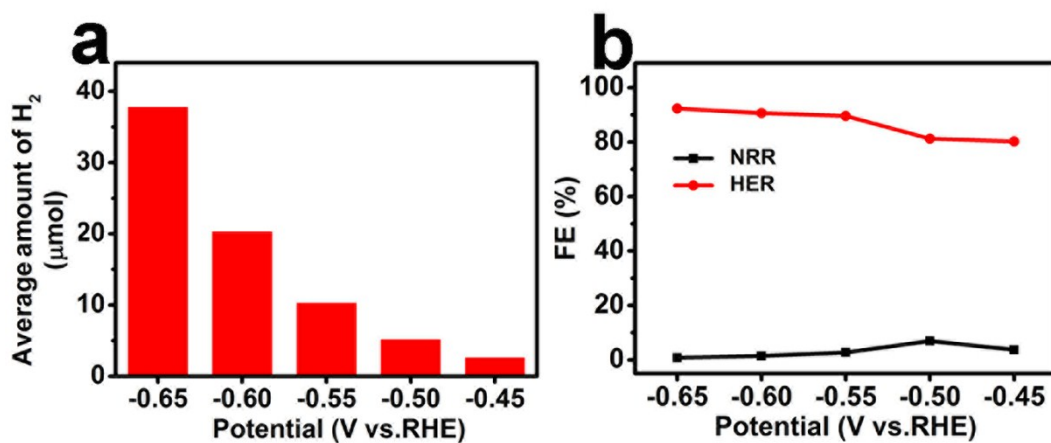


Fig. S5. (a) Amount of evolved H₂ determined by gas chromatography from the headspace of the cell in N₂-saturated 0.1 M HCl at various potentials. (b) The calculated FEs of HER and NRR.

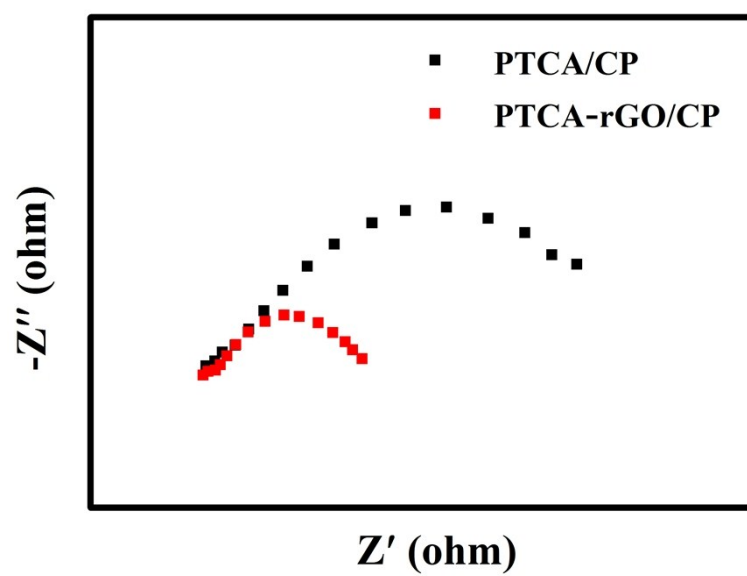


Fig. S6. Nyquist plots of PTCA-rGO/CP and PTCA/CP.

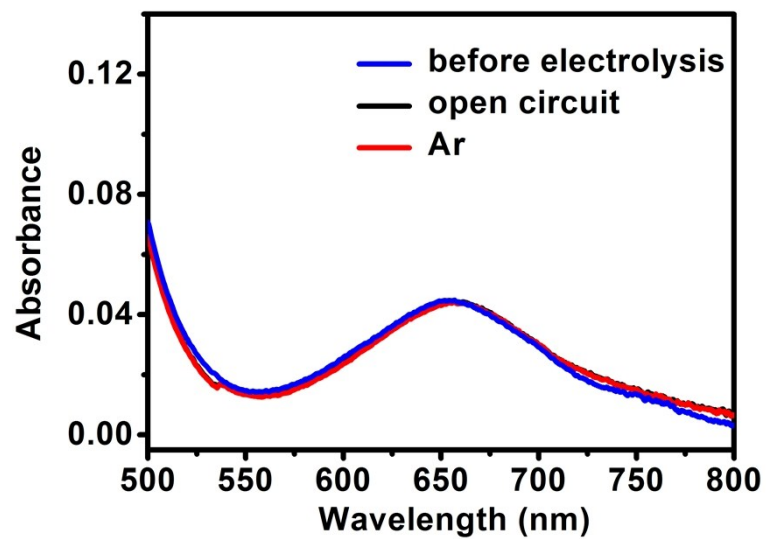


Fig. S7. UV-Vis absorption spectra of the electrolyte stained with indophenol indicator after charging at -0.50 V for 2 h under different electrochemical conditions.

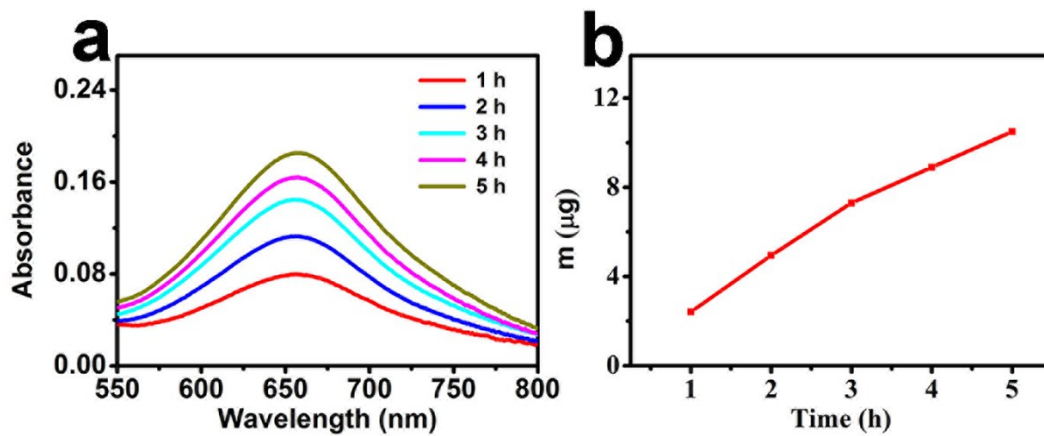


Fig. S8. (a) UV-Vis absorption spectra of the electrolytes stained with indophenol indicator at a -0.50 V after different electrolysis time. (b) The mass of produced NH_3 vs. time recorded at -0.50 V.

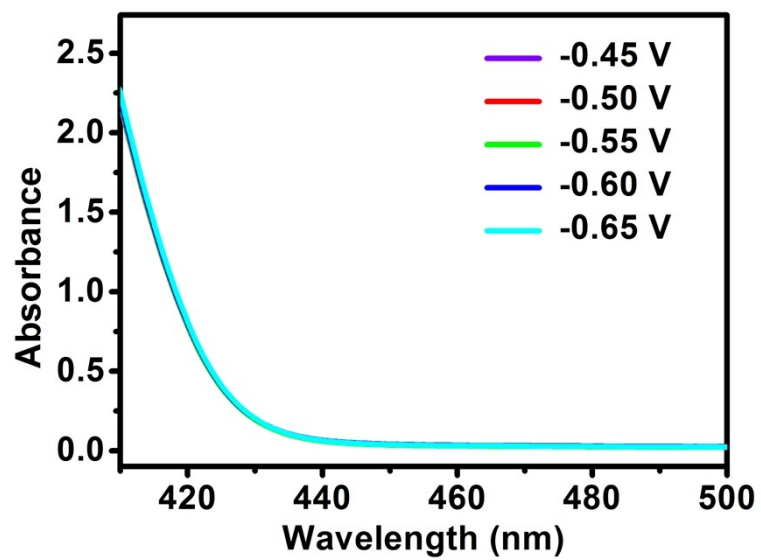


Fig. S9. UV-Vis spectra of the electrolyte estimated by the method of Watt and Chrisp after 2 h electrolysis at a series of potentials under ambient conditions.

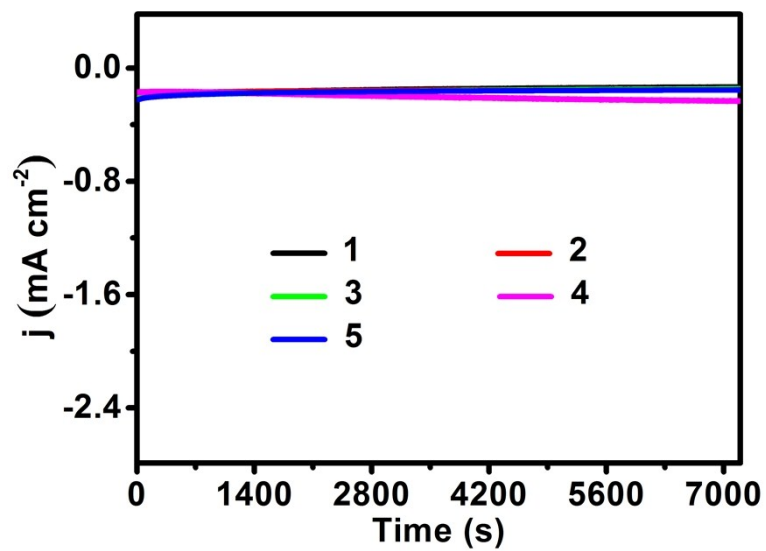


Fig. S10. Time-dependent current density curves of PTCA-rGO/CP at -0.50 V for 5 consecutive cycles.

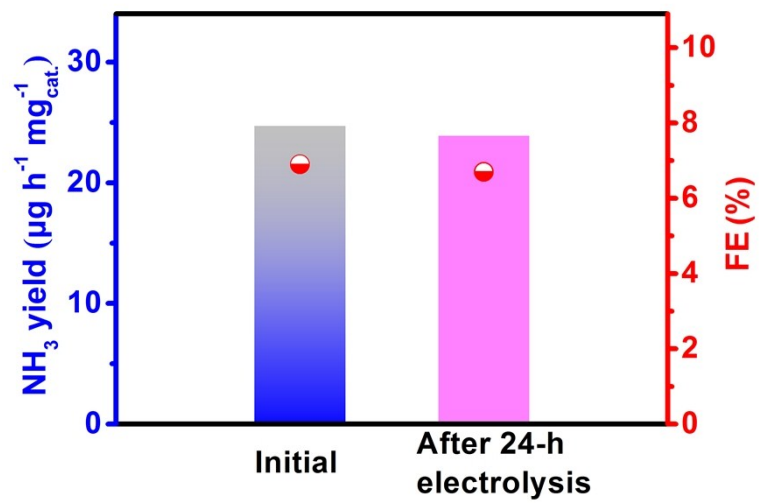


Fig. S11. NH_3 yields and FEs with different PTCA-rGO/CP.

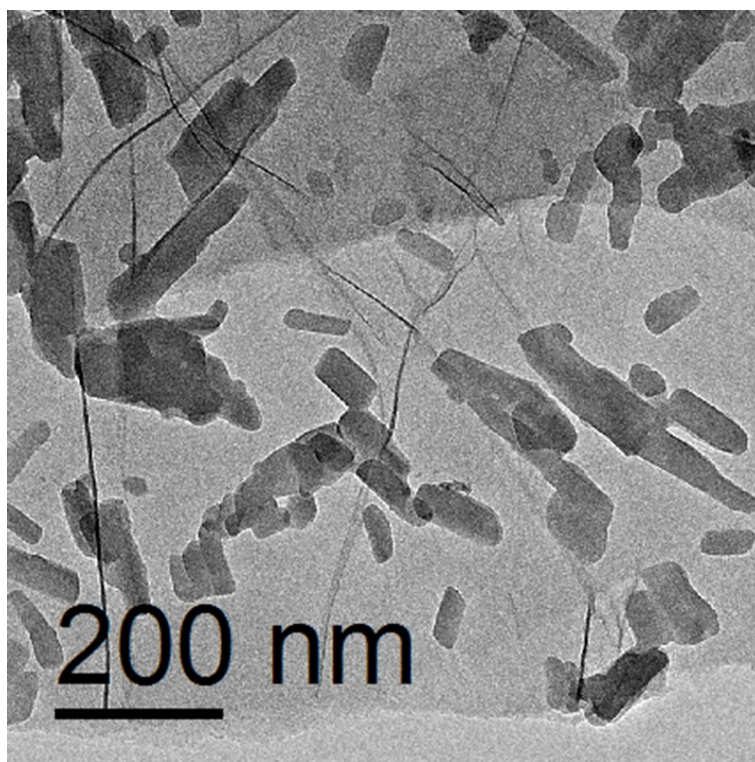


Fig. S12. TEM image of PTCA-rGO after stability test.

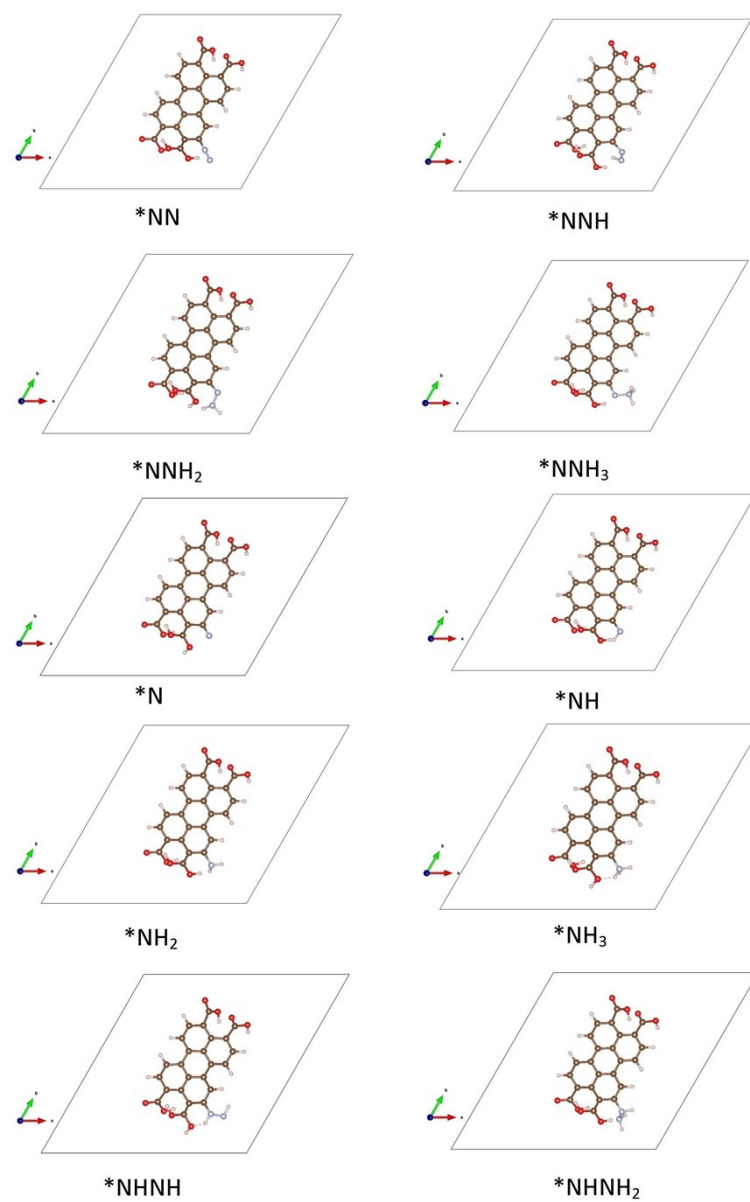


Fig. S13. Reaction steps occurring on the surface of PTCA according to NRR associative mechanism. An asterisk (*) denotes a surface site. Color codes: C, brown; O, red; N, silver; H, light magenta.

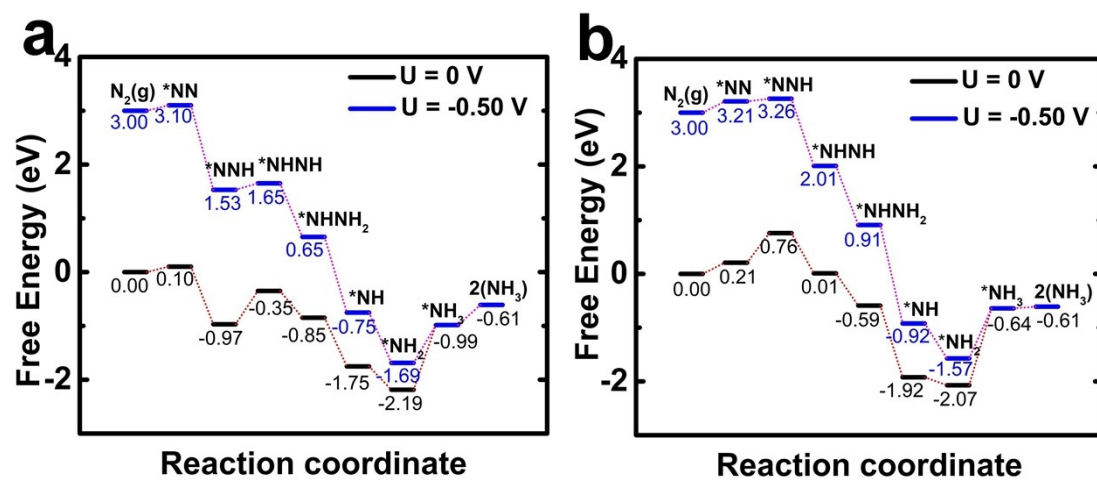


Fig. S14. Free energy diagram for the associative distal mechanism of (a) PTCA-rGO and (b) PTCA when the NRR occurs on PTCA.

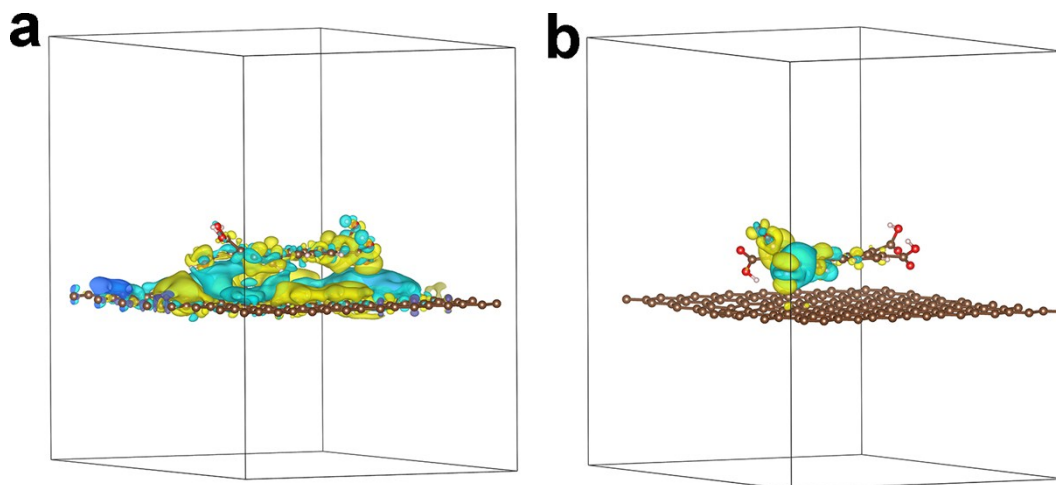


Fig. S15. Differential charge density plottings of (a) $Q_{\text{PTCA-rGO}}-Q_{\text{PTCA}}-Q_{\text{rGO}}$ in PTCA-rGO and (b) $Q_{\text{N}_2\text{-PTCA-rGO}}-Q_{\text{PTCA-rGO}}-Q_{\text{N}_2}$ in N_2 adsorbed on the surface of PTCA-rGO, where the colors of yellow and cyan are labeled the positive and negative charge density, respectively.

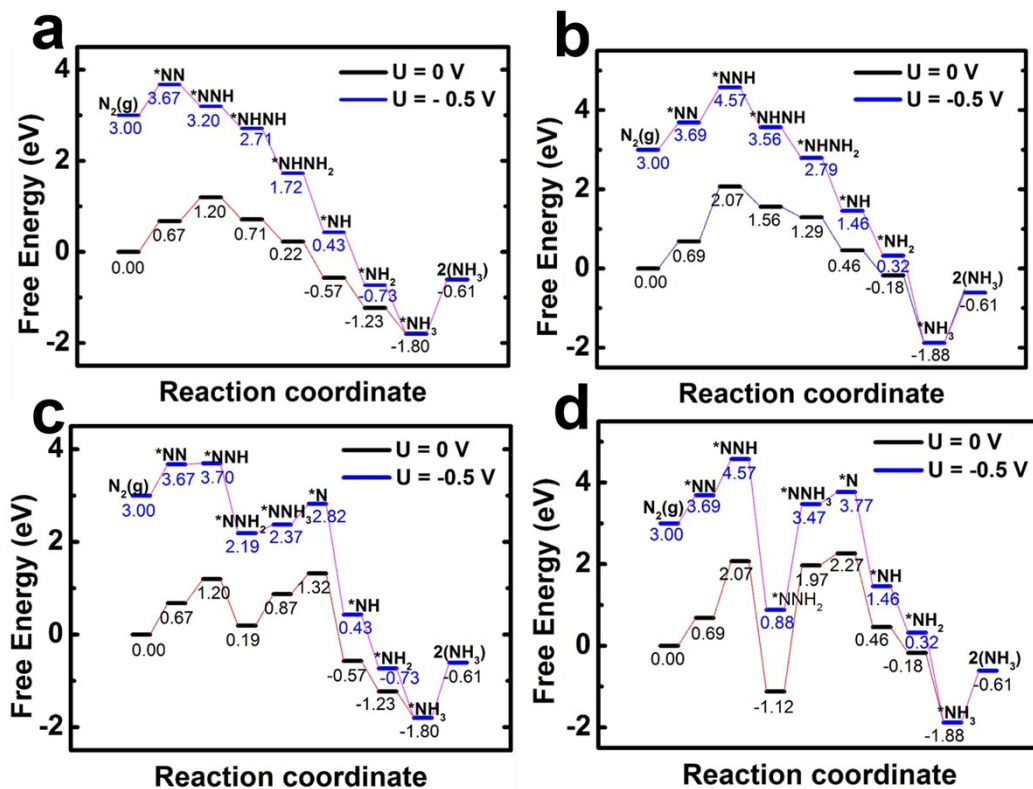


Fig. S16. Free energy diagram for the associative alternating mechanism of (a) PTCA-rGO and (b) rGO when the NRR occurs on rGO. Free energy diagram for the associative distal mechanism of (c) PTCA-rGO and (d) rGO when the NRR occurs on rGO.

Table S1. Comparison of the catalytic performances of PTCA-rGO/CP with other NRR catalysts at ambient conditions.

Catalyst	Electrolyte	NH ₃ yield	FE (%)	Ref.
PTCA-rGO	0.1 M HCl	24.7 $\mu\text{g h}^{-1} \text{mg}^{-1}_{\text{cat}}$	6.9	This work
N-doped hierarchical porous carbon foams	0.1 M HCl	15.7 $\mu\text{g h}^{-1} \text{mg}_{\text{cat}}^{-1}$	1.45	10
O-KFCNTs	0.1 M HCl	25.1 $\mu\text{g h}^{-1} \text{mg}^{-1}_{\text{cat}}$	5.7	11
PCN	0.1 M HCl	8.09 $\mu\text{g h}^{-1} \text{mg}^{-1}_{\text{cat}}$	11.59	12
MoO ₃	0.1 M HCl	29.43 $\mu\text{g h}^{-1} \text{mg}^{-1}_{\text{cat}}$	1.9	13
Bi ₄ V ₂ O ₁₁ /CeO ₂	0.1 M HCl	23.21 $\mu\text{g h}^{-1} \text{mg}^{-1}_{\text{cat}}$	10.16	14
hexagonal boron nitride nanosheet	0.1 M HCl	22.4 $\mu\text{g h}^{-1} \text{mg}^{-1}_{\text{cat}}$	4.7	15
N, P co-doped hierarchical porous carbon	0.1 M HCl	0.97 $\mu\text{g h}^{-1} \text{mg}^{-1}_{\text{cat}}$	4.2	16
NP-C-MOF-5	0.1 M HCl	1.08 $\mu\text{g h}^{-1} \text{mg}^{-1}_{\text{cat}}$	-	17
N-doped porous carbon	0.05 M H ₂ SO ₄	23.8 $\mu\text{g h}^{-1} \text{mg}^{-1}_{\text{cat}}$	1.42	18
γ -Fe ₂ O ₃	0.1 M KOH	0.212 $\mu\text{g h}^{-1} \text{mg}^{-1}_{\text{cat}}$	1.9	19
Au nanorods	0.1 M KOH	1.648 $\mu\text{g h}^{-1} \text{cm}^{-2}$	4	20
Rh nanosheets	0.1 M KOH	23.88 $\mu\text{g h}^{-1} \text{mg}^{-1}_{\text{cat}}$	0.217	21
NCF	0.1 M KOH	15.804 $\mu\text{g h}^{-1} \text{mg}^{-1}_{\text{cat}}$	2.72	22
Pd-Co/CuO	0.1 M KOH	10.04 $\mu\text{g h}^{-1} \text{mg}^{-1}_{\text{cat}}$	2.16	23
CoP hollow nanocage	1.0 M KOH	10.78 $\mu\text{g h}^{-1} \text{mg}^{-1}_{\text{cat}}$	7.36	24
Fe/Fe ₃ O ₄	0.1 M PBS	0.19 $\mu\text{g h}^{-1} \text{cm}^{-2}$	8.29	25
Fe ₂ O ₃ nanorod	0.1 M Na ₂ SO ₄	15.9 $\mu\text{g h}^{-1} \text{mg}^{-1}_{\text{cat}}$	0.94	26
TiO ₂	0.1 M Na ₂ SO ₄	0.56 $\mu\text{g} \cdot \text{h}^{-1} \cdot \text{cm}^{-2}$	2.5	27

Mn ₃ O ₄	0.1 M Na ₂ SO ₄	11.6 μg h ⁻¹ mg ⁻¹ _{cat.}	3.0	28
VO ₂ hollow microsphere	0.1 M Na ₂ SO ₄	14.85 μg h ⁻¹ mg ⁻¹ _{cat.}	3.97	29
S-doped carbon nanosphere	0.1 M Na ₂ SO ₄	19.07 μg h ⁻¹ mg ⁻¹ _{cat.}	7.47	30
defect-rich fluorographene	0.1 M Na ₂ SO ₄	9.3 μg h ⁻¹ mg ⁻¹ _{cat.}	4.2	31
La ₂ O ₃	0.1 M Na ₂ SO ₄	17.04 μg h ⁻¹ mg ⁻¹ _{cat.}	4.76	32
Mn ₃ O ₄ @rGO	0.1 M Na ₂ SO ₄	17.4 μg h ⁻¹ mg ⁻¹ _{cat.}	3.52	33

References

- 1 D. Zhu, L. Zhang, R. E. Ruther and R. J. Hamers, *Nat. Mater.*, 2013, **12**, 836–841.
- 2 G. W. Watt and J. D. Chrisp, *Anal. Chem.*, 1952, **24**, 2006–2008.
- 3 J. P. Perdew, K. Burke and Y. Wang, *Phys. Rev. B*, 1996, **54**, 16533–16539.
- 4 G. Kresse and D. Joubert, *Phys. Rev. B*, 1999, **59**, 1758–1775.
- 5 G. Kresse and J. Hafner, *Phys. Rev. B*, 1993, **47**, 558–561.
- 6 G. Kresse and J. Hafner, *J. Phys. Condens. Matter*, 1994, **6**, 8245.
- 7 G. Kresse, J. Hafner, *Phys. Rev. B*, 1994, **49**, 14251–14269.
- 8 E. Skulason, T. Bligaard, S. Gudmundsdottir, F. Stunt, J. Rossmeisl, F. Abild-Pedersen, T. Vegge, H. Jonsson and J. K. Nørskov, *Phys. Chem. Chem. Phys.*, 2012, **14**, 1235–1245.
- 9 <http://ccbdb.nist.gov/>.
- 10 X. Yang, K. Li, D. Cheng, W. Pang, J. Lv, X. Chen, H. Zang, X. Wu, H. Tan, Y. Wang and Li, Y. *J. Mater. Chem. A*, 2018, **6**, 7762–7769.
- 11 T. Wu, P. Li, H. Wang, R. Zhao, Q. Zhou, W. Kong, M. Liu, Y. Zhang, X. Sun and F. Gong. *Chem. Commun.*, 2019, **55**, 2684–2687.
- 12 C. Lv, Y. Qian, C. Yan, Y. Ding, Y. Liu, G. Chen and G. Yu, *Angew. Chem., Int. Ed.*, 2018, **57**, 10246–10250.
- 13 J. Han, X. Ji, X. Ren, G. Cui, L. Li, F. Xie, H. Wang, B. Li and X. Sun, *J. Mater. Chem. A*, 2018, **6**, 12974–12977.
- 14 C. Lv, C. Yan, G. Chen, Y. Ding, J. Sun, Y. Zhou and G. Yu, *Angew. Chem., Int. Ed.*, 2018, **57**, 6073–6076.
- 15 Y. Zhang, H. Du, Y. Ma, L. Ji, H. Guo, Z. Tian, H. Chen, H. Huang, G. Cui, A. M. Asiri, F. Qu, L. Chen and X. Sun, *Nano Res.*, 2019, **12**, 919–924.

- 16 P. Song, H. Wang, L. Kang, B. Ran, H. Song and R. Wang, *Chem. Commun.*, 2019, **55**, 687–690.
- 17 P. Song, L. Kang, H. Wang, R. Guo, and R. Wang, *ACS Appl. Mater. Interfaces*, 2019, **11**, 12408–12414.
- 18 Y. Liu, Y. Su, X. Quan, X. Fan, S. Chen, H. Yu, H. Zhao, Y. Zhang and J. Zhao, *ACS Catal.*, 2018, **8**, 1186–1191.
- 19 J. Kong, A. Lim, C. Yoon, J. H. Jang, H. C. Ham, J. Han, S. Nam, D. Kim, Y. E. Sung, J. Choi and H. S. Park, *ACS Sustainable Chem. Eng.*, 2017, **5**, 10986–10995.
- 20 D. Bao, Q. Zhang, F. Meng, H. Zhong, M. Shi, Y. Zhang, J. Yan, Q. Jiang and X. Zhang, *Adv. Mater.*, 2017, **29**, 1604799.
- 21 H.-M. Liu, S.-H. Han, Y. Zhao, Y.-Y. Zhu, X.-L. Tian, J.-H. Zeng, J.-X. Jiang, B. Y. Xia and Y. Chen, *J. Mater. Chem. A*, 2018, **6**, 3211–3217.
- 22 L. Cong, Z. Yu, F. Liu and W. Huang, *Catal. Sci. Technol.*, 2019, **9**, 1208–1214.
- 23 W. Fu, Y. Cao, Q. Feng, W. R. Smith, P. Dong, M. Ye and J. Shen, *Nanoscale*, 2019, **11**, 1379–1385.
- 24 W. Guo, Z. Liang, J. Zhao, B. Zhu, K. Cai, R. Zou and Q. Xu, *Small Methods*, 2018, **2**, 1800204.
- 25 L. Hu, A. Khaniya, J. Wang, G. Chen, W. E. Kaden and X. Feng, *ACS Catal.*, 2018, **8**, 9312–9319.
- 26 X. Xiang, Z. Wang, X. Shi, M. Fan and X. Sun, *ChemCatChem*, 2018, **10**, 4530–4535.
- 27 R. Zhang, X. Ren, X. Shi, F. Xie, B. Zheng, X. Guo and X. Sun, *ACS Appl. Mater. Interfaces*, 2018, **10**, 28251–28255.

- 28 X. Wu, L. Xia, Y. Wang, W. Lu, Q. Liu, X. Shi and X. Sun, *Small*, 2018, **14**, 1803111.
- 29 R. Zhang, H. Guo, L. Yang, Y. Wang, Z. Niu, H. Huang, H. Chen, L. Xia, T. Li, X. Shi, X. Sun, B. Li and Q. Liu, *ChemElectroChem*, 2019, **6**, 1014–1018.
- 30 L. Xia, X. Wu, Y. Wang, Z. Niu, Q. Liu, T. Li, X. Shi, A. M. Asiri and X. Sun, *Small Methods*, 2018, **14**, 1800251.
- 31 J. Zhao, J. Yang, L. Ji, H. Wang, H. Chen, Z. Niu, Q. Liu, T. Li, G. Cui and X. Sun, *Chem. Commun.*, 2019, **55**, 4266–4269.
- 32 B. Xu, Z. Liu, W. Qiu, Q. Liu, X. Sun, G. Cui, Y. Wu and X. Xiong, *Electrochim. Acta*, 2019, **298**, 106–111.
- 33 H. Huang, F. Gong, Y. Wang, H. Wang, X. Wu, W. Lu, R. Zhao, H. Chen, X. Shi, A. M. Asiri, T. Li, Q. Liu and X. Sun, *Nano Res.*, 2019, DOI: 10.1007/s12274-019-2352-5.